

Optical transitions in broken gap heterostructures

E. Halvorsen*

Department of Physics, P.O. Box 1048 Blindern, N-0316 Oslo, Norway

Y. Galperin

Department of Physics, P.O. Box 1048 Blindern, N-0316 Oslo, Norway,
and Division of Solid State Physics, Ioffe Physico-Technical Institute of Russian Academy of Sciences,
194021 St. Petersburg, Russia

K. A. Chao

Department of Physics, Lund University, Sölvegatan 14A, S-223 62 Lund, Sweden
(October 25, 2018)

We have used an eight band model to investigate the electronic structures and to calculate the optical matrix elements of InAs-GaSb broken gap semiconductor heterostructures. The unusual hybridization of the conduction band states in InAs layers with the valence band states in GaSb layers has been analyzed in details. We have studied the dependence of optical matrix elements on the degree of conduction-valence hybridization, the tuning of hybridization by varying the width of the GaSb layers and/or InAs layers, and the sensitivity of quantized levels to this tuning. Large spin-orbit splitting in energy bands has been demonstrated. Our calculation can serve as a theoretical modeling for infrared lasers based on broken gap quantum well heterostructures.

73.20.Dx, 78.40.Fy, 78.66.-w

I. INTRODUCTION

The characteristic feature of $\text{Al}_x\text{Ga}_{1-x}\text{Sb}/\text{InAs}$ heterostructures with $x < 0.3$ is the overlap of the InAs conduction band with the $\text{Al}_x\text{Ga}_{1-x}\text{Sb}$ valence band¹. Such systems, often referred to as *broken gap* heterostructures, exhibit interesting negative persistent photoconductivity², semimetal-semiconductor transition induced by magnetic field³, and intrinsic exciton⁴. As the Al concentration increases from $x=0.3$, a staggered band alignment appears at the $\text{Al}_x\text{Ga}_{1-x}\text{Sb}/\text{InAs}$ interface with the valence band edge of $\text{Al}_x\text{Ga}_{1-x}\text{Sb}$ lying in the band gap of InAs. On the other hand, at the GaSb/ $\text{Al}_x\text{Ga}_{1-x}\text{Sb}$ interface the band alignment is of the straddled type. Therefore, in a InAs/ $\text{Al}_x\text{Ga}_{1-x}\text{Sb}/\text{GaSb}$ heterostructure, carriers can tunnel from the InAs conduction band to the GaSb valence through the $\text{Al}_x\text{Ga}_{1-x}\text{Sb}$ barrier.

InAs, GaSb, and AlSb form a family of semiconductors with sufficient lattice match for epitaxy growth. Interband tunneling devices based on the InAs/AlGaSb/GaSb double barrier resonant tunneling have been fabricated, which exhibit high frequency response and peak-to-valley current ratio at room temperatures⁴⁻¹². Because of their potential for technological application, resonant tunneling¹⁴⁻¹⁶ and resonant magnetotunneling¹⁷⁻²⁰ have been

investigated extensively.

To the contrary of tunneling processes, very little work has been done on the electronic structure and optical properties of broken gap heterostructures²³⁻²⁵. We notice that due to the overlap of InAs conduction band and the GaSb valence band, it is possible to form new type of eigenstates with interesting optical properties. We will elaborate this with Fig. 1 where the conduction band edge E_c and the valence band edge E_v are marked for a GaSb/InAs heterostructure embedded in the band gap of AlSb. Treating the AlSb at both sides as potential barriers, the system AlSb/GaSb/InAs/AlSb is essentially a new type of quantum well which we name as broken gap quantum well (BGQW). If we diminish the thickness of either the GaSb layer or the InAs layer to zero, the BGQW reduces to a conventional quantum well which, with bipolar doping becomes a quantum well laser.

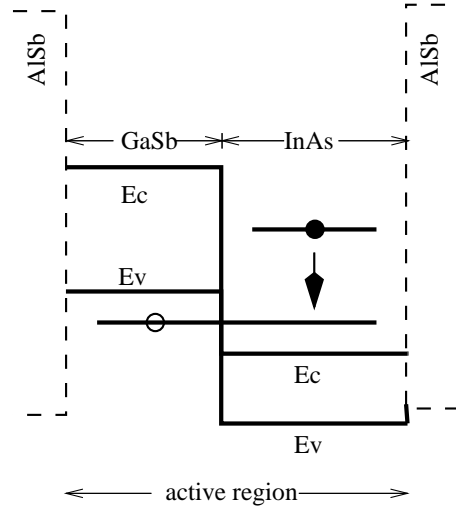


FIG. 1. The possible hybridization between the InAs conduction band states and the GaSb valence band states in the active region of a broken gap quantum well structure provides the novel infrared radiation.

If in a properly designed BGQW there exist two eigenenergies as shown in Fig. 1, under bipolar doping,

the BGQW can lase in the infrared frequency region. Such semiconductor infrared lasers or detectors were proposed earlier^{21,22}. The lower energy state in Fig. 1 is characterized by the degree of hybridization between the GaSb valence band states and the InAs conduction band states. The enhancement of optical transition requires the hybridized wave function having a large amplitude in the InAs layer. On the other hand, to drain out the electrons in the hybridized state in order to achieve the population inversion for lasing, the wave function should have a large component from the GaSb layer. A thorough understanding of this hybridization is important not only for opto-electronic devices, but also for the fundamental theory of transport parallel to interfaces.

The optical property of a BGQW, which is of most theoretical interest and of most importance to optoelectronics, involves the optical transition between these two levels. Hence, relevant issues to be studied are the dependence of optical matrix elements on the degree of conduction-valence hybridization, the tuning of hybridization by varying the width of the GaSb layer, and the sensitivity of quantized levels to this tuning. In this paper we will perform a theoretical calculation of electronic structure and optical matrix elements in order to investigate these items. In Sec. II we present the model system we study and the basic assumptions in our theoretical calculation. Our results for the electronic structure and optical matrix elements are given in Sec. III and Sec. IV respectively, and discussed in Sec. V.

II. MODEL AND THEORY

Our model system shown in Fig. 1 is a GaSb/InAs heterostructure sandwiched between two thick AlSb layers. The growth direction is [001] which defines the z axis. The x axis is along [100] and the y axis is along [010]. This system was studied earlier with a simple two band model²⁶. The essential feature of our model is the existence in BGQW quantized conduction band states in the InAs layer, and hybridized quantum levels in the energy regime where the GaSb valence band overlaps with the InAs conduction band. Therefore, for simplicity we can well assume that the two thick AlSb layers are bulk AlSb. As an illustration, one conduction band level and one hybridized level are plotted in Fig. 1. We will perform band structure calculation for the BGQW shown in Fig. 1. The lattice constants are 6.096 Å for GaSb, 6.058 Å for InAs, and 6.136 Å for AlSb. With such small lattice mismatch, the strain estimated with the deformation potential of these materials is not large enough to modify our conclusion qualitatively. Hence, in our theoretical calculation, strain will be neglected. As will be discussed in Sec. III, the essential feature of our model mentioned above, and hence the conclusion reached by our calculation will remain intact even this weak strain effect is taken into account.

We employ the effective bond orbital model²⁷ (EBOM) which is a tight-binding-like model defined on the Bravais lattice of the underlying crystal. The basis are constructed as linear combinations of orbitals centered on each lattice site having s - or p -symmetry, together with spin eigenstates. The so-constructed basis functions diagonalize the spin-orbit interaction. Our model Hamiltonian includes local and nearest neighbor matrix elements. The degree of inversion asymmetry of the BGQW heterostructure under study is much higher than that of individual InAs or GaSb constituent layers. Hence, in our calculation the effect of weak inversion symmetry is neglected for simplicity. On the other hand, the strong inversion symmetry of the BGQW and its combined effect with the spin-orbit coupling at finite in-plane wavevector are fully taken into account in our theoretical treatment.

It is worthwhile to point out that the EBOM is not an atomistic model like the tight binding model. While the tight binding model is built from orbitals representing the degree of freedom of each individual atom, the bond-orbitals in the EBOM are confined to a primitive unit cell and represent more than one atom. The symmetry of the EBOM is identical to that of the $\mathbf{k}\cdot\mathbf{p}$ model, and therefore in both models there is no asymmetry between the (110) and ($\bar{1}\bar{1}0$) directions. On the other hand, the difference between the EBOM and the $\mathbf{k}\cdot\mathbf{p}$ model is that the $\mathbf{k}\cdot\mathbf{p}$ model is a continuum model without a natural momentum cutoff, but the EBOM is discretized on the Bravais lattice of the crystal.

The bulk parameters of the EBOM, which are required for our calculation, are obtained by fitting the bulk band-structure of EBOM to that of the $\mathbf{k}\cdot\mathbf{p}$ Hamiltonian near the Γ point to the second order in k , as described in Ref 27. The EBOM can therefore be considered as an effective mass theory discretized on the Bravais lattice. For small \mathbf{k} vectors the two models are equivalent. However, since EBOM is discretized on the Bravais lattice, it gives better results at large k . It is important to point out that usually, as in the present case, it is not even necessary to know the precise form of the effective bond orbitals.

Because of the large overlap between the InAs conduction band and the GaSb valence band, the split-off band must be included in our treatment. Hence, we will deal essentially an eight band Kane model. We consider the BGQW heterostructures grown in the [001] direction, with n labelling the (001) planes. Then, the position of a lattice site \vec{R}_n in the n th plane can be expressed as $(n\frac{a}{2}, \vec{R}_n)$, where a is the lattice constant of the conventional unit cell. The eight bond orbitals at each lattice site are conventionally labelled as $(S\frac{1}{2}\frac{1}{2})$, $(S\frac{1}{2}-\frac{1}{2})$, $(P\frac{3}{2}\frac{3}{2})$, $(P\frac{3}{2}\frac{1}{2})$, $(P\frac{3}{2}-\frac{1}{2})$, $(P\frac{3}{2}-\frac{3}{2})$, $(P\frac{1}{2}\frac{1}{2})$, and $(P\frac{1}{2}-\frac{1}{2})$. We denote $|n, \vec{R}_n, \alpha\rangle$ for the α th bond orbital at position $(n\frac{a}{2}, \vec{R}_n)$. In terms of these bond orbitals, we define a basis set of planar orbitals

$$|n, \vec{k}_{\parallel}, \alpha\rangle = N_{\parallel}^{-1/2} \sum_{\vec{R}_n} \exp(i\vec{k}_{\parallel} \cdot \vec{R}_n) |n, \vec{R}_n, \alpha\rangle, \quad (1)$$

where \vec{k}_{\parallel} is an in-plane wave vector, and N_{\parallel} is the number of sites in each plane.

Using this basis of planar orbitals, the Hamiltonian

$$H = \sum_{\vec{k}_{\parallel}} H_{\vec{k}_{\parallel}}$$

is decomposed into a linear combination of partial Hamiltonians $H_{\vec{k}_{\parallel}}$. The partial Hamiltonian

$$H_{\vec{k}_{\parallel}} = \sum_{n\alpha\beta} e_{n, \vec{k}_{\parallel}, \alpha\beta} |n, \vec{k}_{\parallel}, \alpha\rangle \langle n, \vec{k}_{\parallel}, \beta| + \sum_{n\alpha\beta} \left(v_{n, \vec{k}_{\parallel}, \alpha\beta} |n+1, \vec{k}_{\parallel}, \alpha\rangle \langle n, \vec{k}_{\parallel}, \beta| + h.c. \right) \quad (2)$$

is diagonal with respect to the in-plane wave vectors \vec{k}_{\parallel} , and block-tridiagonal with respect to the remaining quantum numbers. This form of Hamiltonian is suitable for numerical computations.

The matrix elements in $H_{\vec{k}_{\parallel}}$, except for those $v_{n, \vec{k}_{\parallel}, \alpha\beta}$ which connect the two bond orbital planes forming an interface, are set to the values for the corresponding bulk materials. At an interface, we follow the commonly accepted approach to determine the value of $v_{n, \vec{k}_{\parallel}, \alpha\beta}$ as the average of the parameter values of the bulk materials on each side of the interface. The materials parameter values from which the effective bond orbital parameters are derived are given in Table I. The valence band offsets are 0.56 eV for GaSb-InAs, 0.18 eV for AlSb-InAs, and -0.38 eV for AlSb-GaSb.

TABLE I. Parameters used to determine effective bond orbital parameters

	InAs	GaSb	AlSb
a (Å)	6.0583	6.082	6.133
E_g (eV)	0.41	0.8128	2.32
m_c/m_0	0.024	0.042	0.18
Δ (eV)	0.38	0.752	0.75
E_P (eV)	22.2	22.4	18.7
γ_1	19.67	11.80	4.15
γ_2	8.37	4.03	1.01
γ_3	9.29	5.26	1.75

For a given \vec{k}_{\parallel} , the eight eigenfunctions

$$|\Psi_{\gamma, \vec{k}_{\parallel}}\rangle = \sum_{n, \alpha} F_{n, \vec{k}_{\parallel}, \alpha}^{\gamma} |n, \vec{k}_{\parallel}, \alpha\rangle; \quad \gamma = 1, 2, \dots$$

and the corresponding band energies $E_{\gamma, \vec{k}_{\parallel}}$ can be readily obtained from Eq. (2) by diagonalizing a finite tridiagonal matrix for a BGQW of finite width. Knowing the eigensolutions, we will calculate the optical matrix elements.

The representation of the momentum operator in the bond-orbital basis contains the leading local and nearest neighbor matrix elements. They are determined by mapping the bulk matrix elements to the $\mathbf{k}\cdot\mathbf{p}$ results up to and including terms linear in wave vector²⁸. In the planar orbital basis, its \vec{k}_{\parallel} -diagonal part can be expressed as

$$P^{\nu}(\vec{k}_{\parallel}) = \sum_{n\alpha\beta} P_{n, \vec{k}_{\parallel}, \alpha\beta}^{\nu} |n, \vec{k}_{\parallel}, \alpha\rangle \langle n, \vec{k}_{\parallel}, \beta| + \sum_{n\alpha\beta} \left(Q_{n, \vec{k}_{\parallel}, \alpha\beta}^{\nu} |n+1, \vec{k}_{\parallel}, \alpha\rangle \langle n, \vec{k}_{\parallel}, \beta| + h.c. \right), \quad (3)$$

where $\nu=x, y, z$ is the polarization direction. The matrix elements are

$$P_{n, \vec{k}_{\parallel}, \alpha\beta}^{\nu} = \sqrt{\frac{2}{m_0}} \langle n, \vec{k}_{\parallel}, \alpha | p_{\nu} | n, \vec{k}_{\parallel}, \beta \rangle, \quad (4)$$

$$Q_{n, \vec{k}_{\parallel}, \alpha\beta}^{\nu} = \sqrt{\frac{2}{m_0}} \langle n+1, \vec{k}_{\parallel}, \alpha | p_{\nu} | n, \vec{k}_{\parallel}, \beta \rangle, \quad (5)$$

where m_0 is the free electron mass. In the above matrix elements we have included the prefactor $\sqrt{2/m_0}$ such that these matrix elements have units $(eV)^{1/2}$.

III. ELECTRONIC STRUCTURE

In the following we will examine the electronic structure of the InAs-GaSb BGQW shown in Fig. 1. Before the InAs layers and the GaSb layers are coupled together, we will denote the n th electronic levels in the conduction band by E_n , the n th energy levels in the heavy-hole band by H_n , and the n th energy levels in the light-hole band by L_n . Such conventional labeling is unambiguous for $\vec{k}_{\parallel}=0$.

The symmetry properties of EBOM at $\vec{k}_{\parallel}=0$ allows the conduction band states in the InAs layers to hybridize with the light-hole band states in the GaSb layers, but not with the heavy-hole band states. We would like first to locate the region of BGQW structures in which we can fine tune the degree of such hybridization. For this purpose, we perform two energy level calculations; one with zero InAs layer width and the other with zero GaSb layer width. The results are plotted in Fig. 2 as functions of the number of atomic layers. We see that for 58 atomic layers, the GaSb L1 level overlaps with the InAs E1 level. Hence, the region around 60 atomic layers will be the reasonable starting BGQW structure for tuning the system into maximum hybridization. We should be aware of the fact that different confinement boundary conditions also affect the degree of hybridization, as will be seen in our computed results below.

We will then set 60 atomic layers for the InAs constituent and vary the GaSb width from 30 to 80 atomic layers. In the absence of interface coupling, the H1, E1, H2 and L1 levels at $\vec{k}_{\parallel}=0$ are shown in Fig. 3 as dashed

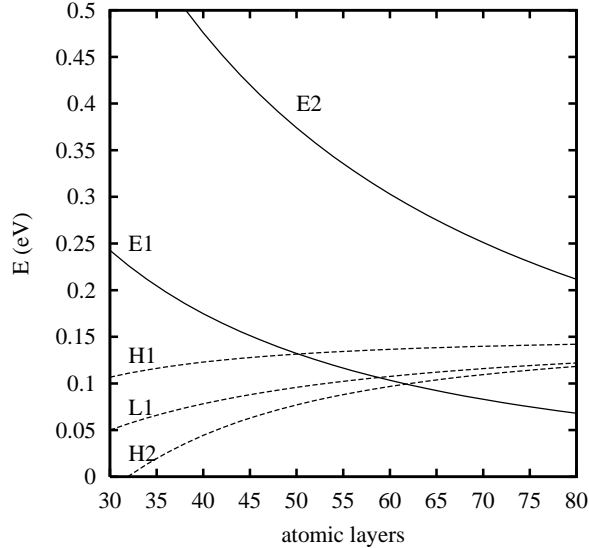


FIG. 2. Electron energies in a AlSb-InAs-AlSb quantum well (solid curves), and in a AlSb-GaSb-AlSb quantum well (dashed curves) as functions of well width. All energies are measured from the InAs conduction band edge.

curves (hole states are the same as in Fig. 2). In the BGQW sample with 80 atomic layers of GaSb, these four levels are ordered as $H1 > L1 > H2 > E1$. When the interface coupling is turned, these four levels are shown in Fig. 3 as solid curves. For the convenience of description, we use the results at 80 atomic layers of GaSb to label them as $H1 > E1 > H2 > L1$. Because of the symmetry properties at $\vec{k}_{\parallel}=0$, the conduction band states have negligible influence on H1 and H2 levels. The heavy hole levels are only slightly perturbed by the change of boundary conditions. On the other hand, the L1 and E1 levels are strongly hybridized and repel each other. The difference between the solid curves and the dashed curves is also due to the different confinement boundary conditions as mentioned above. In the region of GaSb width between 50 and 60 atomic layers, the separation of the two resulting hybridized levels is about 40-55 meV.

To demonstrate the spatial properties of hybridized states, we have calculated the real space occupation probability

$$\mathcal{O}_n^{\gamma}(\vec{k}_{\parallel}=0) \equiv \sum_{\alpha} |F_{n,\vec{k}_{\parallel}=0,\alpha}^{\gamma}|^2; \quad \gamma = 1, 2, \dots$$

$\mathcal{O}_n^{\gamma}(\vec{k}_{\parallel}=0)$ of five eigenstates in a BGQW with 56 GaSb atomic layers and 60 InAs atomic layers are plotted in Fig. 4. From top to bottom, the first state is E2 which is largely confined in InAs layers. The second and fourth state, which localized in GaSb layers, are H1 and H2 respectively. The third and the lowest states are E1-L1 hybridized states. To be consistent with our earlier convention, the third state is E1, and the lowest state is L1.

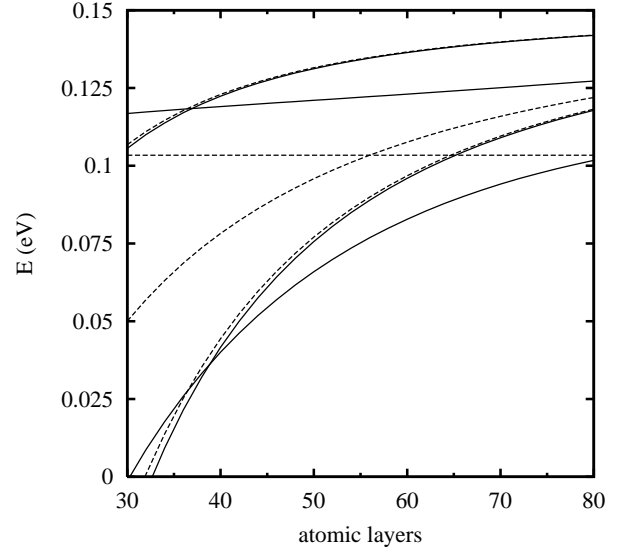


FIG. 3. Zone center ($\vec{k}_{\parallel}=0$) H1, H2, L1, and E1 levels as functions of GaSb layer width in a InAs-GaSb BGQW with 60 InAs atomic layers. Dashed curves are for the case without the InAs-GaSb interface coupling (ordered as $H1 > L1 > H2 > E1$ at 80 atomic layers of GaSb), and the solid curves are for the case with the InAs-GaSb interface coupling (for convenience, ordered as $H1 > E1 > H2 > L1$ at 80 atomic layers of GaSb).

One way to further analyze this issue is to decompose the total occupation probability into partial occupation probability for each α band. Such decomposition is shown in Fig. 5 with dotted curves for the E1 state, and the solid curves for the L1 state. In this figure, the two upper plots are for the $P_{\frac{3}{2},\pm\frac{1}{2}}$ components and the two lower plots are for the $S_{\frac{1}{2},\pm\frac{1}{2}}$ components. We see that the tail of the E1 (or L1) state in the GaSb (or InAs) region has the same component profile as its main part in the InAs (or GaAs) region. Such features were also obtained for InAs-GaSb superlattices in a very recent paper²⁵.

In our derivation of the eigensolutions of a BGQW heterostructure, the effect of strain has been neglected. The separations between the so-obtained eigenenergies for $\vec{k}_{\parallel}=0$, which are determined by the confinement potential, are substantially larger than the energy shifts produced by the strain. Hence, even the effect of strain is included in an improved calculation, the formation of E1-L1 hybridized states is still dominated by the confinement potential, and the degree of hybridization can still be tuned by changing the width of the GaSb and/or the InAs layers. In this respect, the conclusion reached with our present calculation will remain intact when the effect of strain is taken into account.

An interesting question is, when a charge carrier occupies a E1-L1 hybridized state, will its physical properties electron-like or hole-like? For example, what will be the

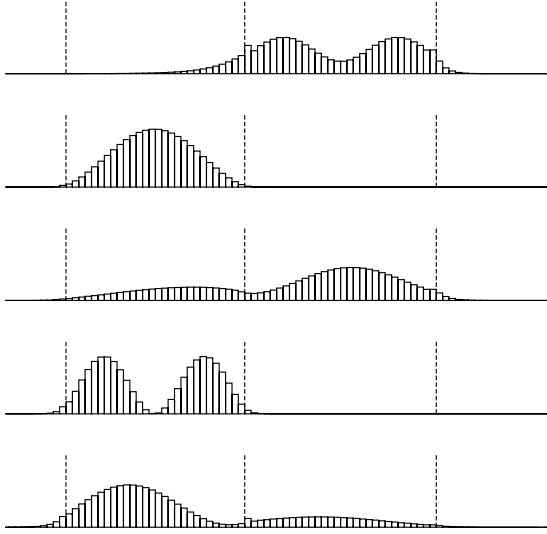


FIG. 4. Real space occupation probability of five zone center ($\vec{k}_{\parallel}=0$) eigenstates in the active region of a BGQW with 56 GaSb atomic layers and 60 InAs atomic layers.

cyclotron effective mass of such a charge carrier? One relevant quantity is the probability

$$\mathcal{O}_{\text{InAs}}^{\gamma}(\vec{k}_{\parallel}=0) \equiv \sum_{n \in \text{InAs}} \mathcal{O}_n^{\gamma}(\vec{k}_{\parallel}=0); \quad \gamma = 1, 2, \dots$$

to find the electron in InAs layers when it occupies the γ th eigenstate. For the two hybridized states (labeled as E1 and L1 in our convention) in a InAs-GaSb BGQW with 60 InAs atomic layers, the results are plotted in Fig. 6 as function of the number of GaSb atomic layers. The solid curves are for $\mathcal{O}_{\text{GaSb}}^{\gamma}(\vec{k}_{\parallel}=0)$, and the dashed curves are for $\mathcal{O}_{\text{InAs}}^{\gamma}(\vec{k}_{\parallel}=0)$. For thin GaSb layers, the charge carrier in a hybridized state is mostly either electron-like or hole-like. However, as the width of GaSb layers increases towards 80 atomic layers, the characteristic features of the charge carrier remain to be studied.

The above calculations for zone center ($\vec{k}_{\parallel}=0$) states are repeated for finite \vec{k}_{\parallel} , and the dispersion relations of various subbands are shown in Fig. 7 for a BGQW with 60 InAs atomic layers and 60 GaSb atomic layers. We have chosen \vec{k}_{\parallel} along the [100] direction, or the x axis. At zone center, from top to bottom the levels are E2, H1, E1, H2, L1, and L2. In region of finite \vec{k}_{\parallel} , the spin-splitting of levels and the anticrossing of levels are clearly seen. We will return to these dispersion relations later for further discussions.

We have mentioned that our BGQW system was studied earlier with a simple two-band model²⁶, where only the H1 and the E1 levels are included. Therefore, in Ref. 26 there is no E1-L1 hybridization. The energy bands shown in Fig. 2 of Ref. 26 corresponds to our E1

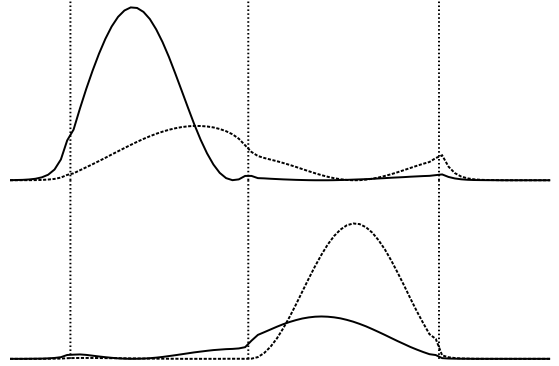


FIG. 5. Structure of the states L1 (solid curves) and E1 (dotted curves), with the two upper plots for the $P_{\frac{3}{2}, \pm \frac{1}{2}}$ components and the two lower plots for the $S_{\frac{1}{2}, \pm \frac{1}{2}}$ components.

and H1 bands in Fig. 7, within the region $0 < ka < 0.12$. The two-band calculation does yield an anticrossing at finite \vec{k}_{\parallel} , but gives no spin-orbit splitting.

IV. OPTICAL MATRIX ELEMENTS

Knowing the eigenfunctions of the BGQW heterostructure, the optical matrix elements are readily calculated with Eq. (3). Because for finite \vec{k}_{\parallel} each dispersion curve is spin-orbit split into two curves, we distinguish them as E_{na} and E_{nb} for conduction band states, H_{na} and H_{nb} for heavy-hole band states, and L_{na} and L_{nb} for light-hole band states. For convenience, in the region of small \vec{k}_{\parallel} , the lower spin-orbit split dispersion curve is assigned with a, and the higher one with b.

There are numerous optical transitions between each pair of states for different polarizations of the electromagnetic waves. The selection rules are complicated by the anticrossing of levels as well as the hybridization between InAs conduction band states and GaSb valence band states. Hence, here our study will focus on the cases of our interest: the optical transitions from the E2a and E2b levels to the E1a, E1b, H1a, and H1b levels. As will be discussed later, such transitions are relevant to the possible infrared lasers based on BGQW heterostructures. We would like to mention that parallel to our work, in a very recent paper²⁵, in InAs-GaSb superlattices the optical transition matrix elements at $\vec{k}_{\parallel}=0$ with in-plane polarization were studied as functions of the superlattice period.

By analyzing our extensive numerical results, we have reached the following selection rules for transitions from the E2a and E2b levels to the E1a, E1b, H1a, and H1b levels. For \vec{k}_{\parallel} in the [100] or the [110] direction, among the two transitions from E2a (or E2b) to E1a or E1b, only one is allowed. Similarly, among the two transitions

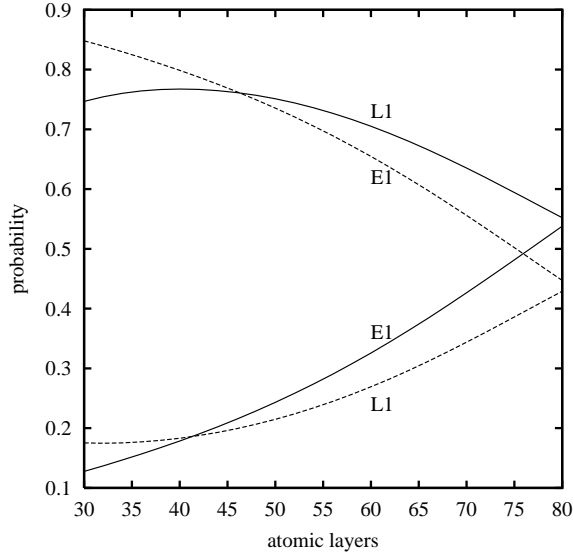


FIG. 6. Probabilities of finding an electron in the GaSb layers (solid lines) or in the InAs layers (dashed lines) as function of GaSb layer width, when the electron occupies the hybridized states E1 or L1 in a BGQW with 60 InAs atomic layers.

from E2a (or E2b) to H1a or H1b, only one is allowed. However, if \vec{k}_{\parallel} is along a low symmetry direction in the two-dimensional Brillouin zone, such as [210] for example, all transitions are allowed. It is worthwhile to point out that these selection rules for a BGQW, which is asymmetric, happen to be the same as the selection rules for the intersubband transitions in a symmetric conduction band quantum well, derived with a simplified eight band model²⁹.

The numerical results to be discussed below are obtained for a BGQW with 60 InAs atomic layers and 60 GaSb atomic layers, the band structure of which is given in Fig. 7. From Fig. 6 we see a significant E1-L1 hybridization in this BGQW heterostructure. The square of the amplitude of optical matrix elements with z -polarization are shown in Fig. 8. At $\vec{k}_{\parallel}=0$, the optical matrix element is zero for the E2 \rightarrow H1 transition, but is large for the E2 \rightarrow E1 transition, as expected from the symmetry properties. As \vec{k}_{\parallel} increases, the anticrossing between the E1 band and the H1 band occurs around $\vec{k}_{\parallel}a \simeq 0.75$. Consequently, the E2 \rightarrow E1 transition drops sharply to zero, while the E2 \rightarrow H1 transition picks up its strength rapidly.

By changing the polarization of the electromagnetic wave and repeating the calculations of optical matrix elements, the results for y -polarization is shown in Fig. 9 and for x -polarization in Fig. 10. The strength of these transitions are substantially smaller than those for the z polarization, by about two orders of magnitude. The strong wavevector dependence of the optical matrix el-

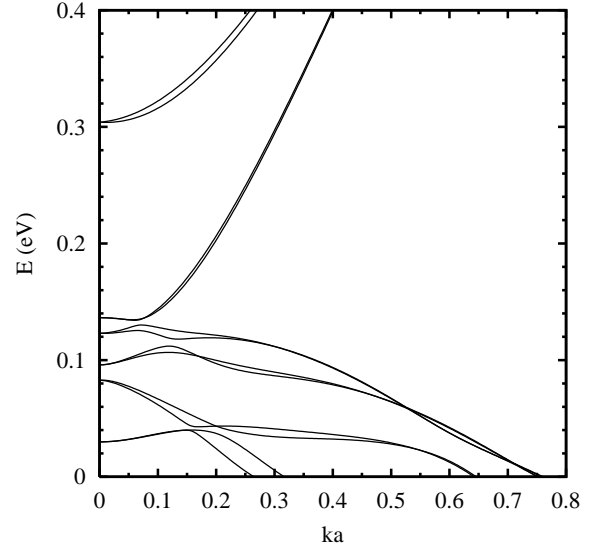


FIG. 7. Subband dispersion with \vec{k}_{\parallel} along [100] direction for an InAs-GaSb BGQW with 60 InAs atomic layers and 60 GaSb atomic layers.

ements in Figs. 9 and 10 is due to the combined effect of spin-orbit splitting and anticrossing of energy bands. The drastic difference between the curves in Fig. 9 and the corresponding curves in Fig. 10 indicates the strong anisotropy of the optical matrix elements with respect to in-plane polarizations.

V. DISCUSSION

The very unusual feature of the BGQW heterostructures is the new eigenstates formed by the hybridization of conduction band states at one side of the interface with the valence band states at the other side. We made a thorough investigation on the formation of such states and their influence on the optical properties of a BGQW. However, their influence on the transport properties parallel to interfaces is perhaps a more important issue for fundamental study. If one tunes the the system to have the Fermi energy lying in a conduction-valence hybridized two-dimensional energy band, depending on the degree of hybridization, the parallel transport properties can change from completely electron-like to complete hole-like.

Another relevant issue for fundamental study is the spin-orbit splitting. Recently, there has been much interest in the effect of spin-orbit interactions in two-dimensional electron gases. For example, the Shubnikov-de Haas measurements of spin-orbit splitting have been performed on symmetric InAs/GaSb³⁰ quantum wells and on symmetric InAs/AlSb³¹ quantum wells, in which the origin of spin-orbit interaction is the lack of inversion

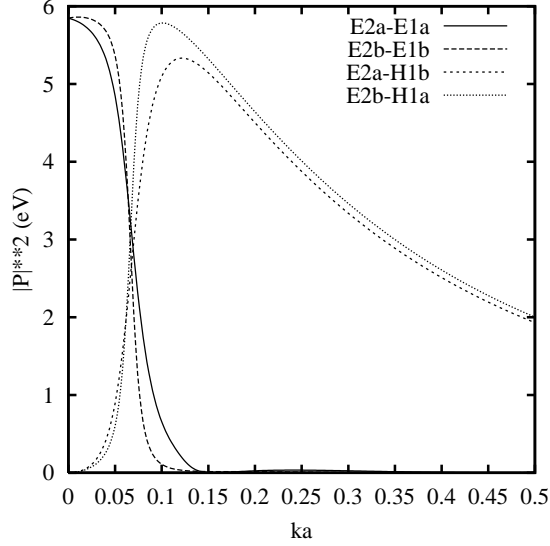


FIG. 8. Square of the amplitude of optical matrix elements with z -polarization as functions of \vec{k}_{\parallel} which is along x axis, for a BGQW with 60 InAs atomic layers and 60 GaSb atomic layers.

symmetry in bulk crystal structure. Because of the asymmetry of the BGQW itself, very large spin-orbit splittings appear in the energy bands as shown in Fig. 7. Consequently, BGQW heterostructures are good candidate for investigating phenomena which are related to spin-orbit interaction.

BGQW heterostructures have great potential in technological applications for lasers and detectors, tunable in infrared wavelengths^{32,33}. Our calculations can serve as the theoretical modeling of such infrared lasers. To make a bipolar laser similar to the conventional quantum lasers, in Fig. 1 the AlSb layers at the InAs side should be n -doped, and the AlSb layers at the GaSb side should be p -doped. The number of InAs atomic layers should be around 60, and the number of GaSb atomic layers should be between 70 and 80. Then, from Fig. 6 we see a strong E1-L1 hybridization. By adjusting the acceptor concentration, we can set the Fermi level between the E1 level and the H2 level shown in Fig. 4. When such BGQW heterostructure is connected to external circuit, electrons which are injected into the E2 energy band will relax to the zone center and make radiation transitions to the E1 band due to the large optical matrix elements of z -polarized light. Then, the strong conduction-valence hybridization of the E1 band states provides the rapid draining of electrons from the E1 band into external circuit via the GaSb valence band states. From Fig. 7 we estimate the energy of emitted photons to be 0.18-0.2 eV, corresponding to wavelength about 6 micrometers. Around this wavelength there exist infrared windows, and consequently such radiation source will be

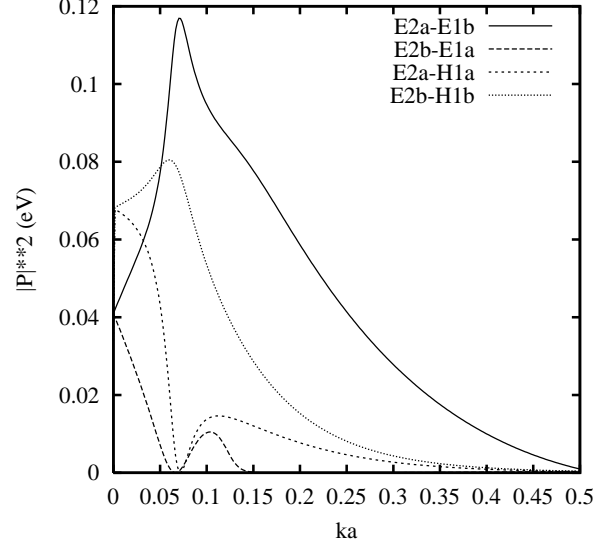


FIG. 9. Same as Fig. 8 but with y -polarization of the electromagnetic wave.

extremely useful.

To close this paper, we must mention the very recent work of Ref. 25 in which the electronic structure and optical matrix elements at the zone center ($\vec{k}_{\parallel}=0$) of InAs-GaSb superlattices have been calculated with both a plane wave pseudopotential method and the eight band $\mathbf{k}\cdot\mathbf{p}$ method. In that paper the effects of superlattice period on various physical quantities at zone center were studied in details. In particular, the authors of Ref. 25 found a zone center E1-H1 coupling manifested by band anticrossing at superlattice period $n=28$, as well as a zone center L1-H2 coupling and anticrossing around $n=13$. Such features are absent in the $\mathbf{k}\cdot\mathbf{p}$ method because it fails to recognize the atomistic details in no-common-atom superlattice. How these features will affect quantitatively the 2D dispersion relation, and hence our results of the formation of E1-L1 hybridization and the in-plane physical properties of a single BGQW heterostructure, as well as their impact on the theoretical modeling of infrared lasers and detectors, remains to be an open question.

ACKNOWLEDGMENTS

This work was supported by the Norwegian Research Council (NFR) under grant no. 111071/431.

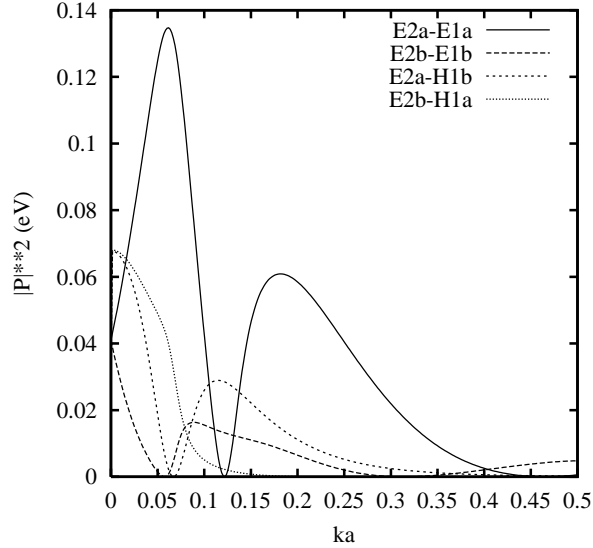


FIG. 10. Same as Fig. 8 but with x -polarization of the electromagnetic wave.

* Present Address: Alcatel Space Norway AS, P.O. Box 138, N-3191 Horten, Norway.

- ¹ H. Munekata, J. C. Maan, L. L. Chang, and L. Esaki, *J. Vac. Sci. Technol. B* **5**, 809 (1987).
- ² G. Tuttle, H. Kroemer, and J. H. English, *J. Appl. Phys.* **65**, 5239 (1989); P. F. Hopkins, A. J. Rimberg, R. M. Westervelt, G. Tuttle, and H. Kroemer, *Appl. Phys. Lett.* **58**, 1428 (1991); Ikai Lo, W. C. Mitchel, M. O. Manasreh, C. E. Stutz, and K. R. Evans, *Appl. Phys. Lett.* **60**, 751 (1992); J.-P. Cheng, Ikai Lo, and W. C. Mitchel, *J. Appl. Phys.* **76**, 667 (1994); Ikai Lo, W. C. Mitchel, S. Elhamri, R. S. Newrock, and R. Kaspi, *Appl. Phys. Lett.* **65**, 1024 (1994).
- ³ T. P. Smith III, H. Nunekata, L. L. Chang, F. F. Fang, and L. Esaki, *Surf. Sci.* **196**, 687 (1998); Ikai Lo, W. C. Mitchel, and J.-P. Cheng, *Phys. Rev. B* **48**, 9118 (1993).
- ⁴ J. Kono, B. D. McCombe, J.-P. Cheng, Ikai Lo, W. C. Mitchel, and C. E. Stutz, *Phys. Rev. B* **50**, 12 242 (1994); J.-P. Cheng, J. Kono, B. D. McCombe, Ikai Lo, W. C. Mitchel, and C. E. Stutz, *Phys. Rev. Lett.* **74**, 450 (1995).
- ⁵ M. Sweeny and J. Xu, *Appl. Phys. Lett.* **54**, 546 (1989).
- ⁶ J. R. Söderström, D. H. Chow, and T. C. McGill, *Appl. Phys. Lett.* **55**, 1094 (1989).
- ⁷ L. F. Luo, R. Beresford, and W. I. Wang, *Appl. Phys. Lett.* **55**, 2023 (1989).
- ⁸ R. Beresford, L. F. Luo, and W. I. Wang, *Appl. Phys. Lett.* **56**, 551 (1990).
- ⁹ R. Beresford, L. F. Luo, K. F. Longenbach, and W. I. Wang, *Appl. Phys. Lett.* **56**, 952 (1990).
- ¹⁰ D. A. Collins, E. T. Yu, Y. Rajakarunanayake, J. R. Söderström, D. Z.-Y. Ting, D. H. Chow, and T. C. McGill, *Appl. Phys. Lett.* **57**, 683 (1990).
- ¹¹ D. Z.-Y. Ting, D. A. Collins, E. T. Yu, D. H. Chow, and T. C. McGill, *Appl. Phys. Lett.* **57**, 1257 (1990).
- ¹² L. Yang, J. F. Chen, and A. Y. Cho, *J. Appl. Phys.* **68**, 2997 (1990).

- ¹³ D. Z.-Y. Ting, E. T. Yu, and T. C. McGill, *Phys. Rev. B* **45**, 3583 (1992).
- ¹⁴ E. E. Mendez, J. Nocera, and W. I. Wang, *Phys. Rev. B* **45**, 3910 (1992).
- ¹⁵ M. S. Kiledjian, J. N. Schulman, K. L. Wang, and K. V. Rousseau, *Phys. Rev. B* **46**, 16 012 (1992).
- ¹⁶ Maria A. Davidovich, E. V. Anda, C. Tejedor, and G. Platero, *Phys. Rev. B* **47**, 4475 (1993).
- ¹⁷ E. E. Mendez, H. Ohno, L. Esaki, and W. I. Wang, *Phys. Rev. B* **43**, 5196 (1991).
- ¹⁸ R. R. Marquardt, D. A. Collins, Y. X. Liu, D. Z.-Y. Ting, and T. C. McGill, *Phys. Rev. B* **53**, 13 624 (1996).
- ¹⁹ Y. X. Liu, R. R. Marquardt, D. Z.-Y. Ting, and T. C. McGill, *Phys. Rev. B* **55**, 7073 (1997).
- ²⁰ A. Zakharova, *J. Phys.: Condens. Matter* **11**, 4675 (1999).
- ²¹ R. Q. Yang and J. M. Xu, *Appl. Phys. Lett.* **59**, 181 (1991).
- ²² H. Ohno, L. Esaki, and E. E. Mendez, *Appl. Phys. Lett.* **60**, 3153 (1992).
- ²³ Yia-Chung Chang and J. N. Schulman, *Phys. Rev. B* **31**, 2069 (1985).
- ²⁴ Ikai Lo, Jih-Chen Chiang, Shioh-Fon Tsay, W. C. Mitchel, M. Ahoujja, R. Kaspi, S. Elhamri, and R. S. Newrock, *Phys. Rev. B* **55**, 13 677 (1997).
- ²⁵ L.-W. Wang, S.-H. Wei, T. Mattila, A. Zunger, I. Vurgaftman, and J. R. Meyer, *Phys. Rev. B* **60**, 5590 (1999).
- ²⁶ Y. Naveh and B. Laikhtman, *Appl. Phys. Lett.* **66**, 1980 (1995).
- ²⁷ Y.-C. Chang, *Phys. Rev. B* **37**, 8215 (1988).
- ²⁸ Y.-C. Chang, *J. Appl. Phys.* **68**, 4233 (1990).
- ²⁹ R. Q. Yang, J. M. Xu, and M. Sweeney, *Phys. Rev. B* **50**, 7474 (1994).
- ³⁰ J. Luo and P. J. Stiles, *Phys. Rev. B* **41**, 7685 (1990).
- ³¹ J. P. Heida, B. J. van Wees, J. J. Kuipers, and T. M. Klapwijk, *Phys. Rev. B* **57**, 11911 (1998).
- ³² R. M. Biefeld, A. A. Allerman, S. R. Kurtz, *Mater. Sci. Eng., B* **51**, 1 (1998).
- ³³ J. R. Meyer, L. J. Olafsen, E. H. Aifer, W. W. Bewley, C. L. Felix, I. Vurgaftman, M. J. Yang, L. Goldberg, D. Zhang, C. H. Lin, S. S. Pei, and D. H. Chow, *IEEE Proc.: Optoelectron.* **145**, 275 (1998).